Pharmacological Research 194 (2023) 106836

Contents lists available at ScienceDirect

Pharmacological Research

journal homepage: www.elsevier.com/locate/yphrs

# Inhibition of CXXC5 function rescues Alzheimer's disease phenotypes by restoring Wnt/β-catenin signaling pathway

Minguen Yoon [a], Heejene Kim [a], Heewon Shin [b], HeeYang Lee [b], Min-Jeong Kang [d], Sung-Hye Park [c], Gyoonhee Han [a], YoungSoo Kim [b,*], Kang-Yell Choi [a,d,**]

[a] Department of Biotechnology, College of Life Science and Biotechnology, Yonsei University, Seoul 03722, Republic of Korea
[b] Department of Pharmacy and Yonsei Institute of Pharmaceutical Sciences, College of Pharmacy, Yonsei University, Incheon 21983, Republic of Korea
[c] Department of Pathology, Seoul National University College of Medicine, Seoul 03080, Republic of Korea
[d] CK Regeon Inc, Seoul 03722, Republic of Korea

ARTICLE INFO

*Keywords:*
Alzheimer's disease
5xFAD
Wnt/β-catenin signaling pathway
CXXC5
*Cxxc5*$^{-/-}$/5xFAD mice
CXXC5-Dvl protein-protein interaction

ABSTRACT

Alzheimer's disease (AD) is the most prevalent type of dementia and is characterized by cognitive deficits and accumulation of pathological plaques. Owing to the complexity of AD development, paradigms for AD research and drug discovery have shifted to target factors that mediate multiple pathogenesis in AD. Increasing evidence suggests that the suppression of the Wnt/β-catenin signaling pathway plays substantial roles in AD progression. However, the underlying mechanism for the suppression of Wnt/β-catenin pathway associated with AD pathogenesis remains unexplored. In this study, we identified that CXXC5, a negative feedback regulator of the Wnt/β-catenin pathway, was overexpressed in the tissues of AD patients and 5xFAD transgenic mice paired with the suppression of Wnt/β-catenin pathway and its target genes related to AD. The level of CXXC5 was upregulated, upon aging of 5xFAD mice. AD characteristics including cognitive deficits, amyloid-β (Aβ) plaques, neuronal inflammation, and age-dependent increment of AD-related markers were rescued in *Cxxc5*$^{-/-}$/5xFAD mice. 5-methoxyindirubin-3'-oxime (KY19334), a small molecule that restores the suppressed Wnt/β-catenin pathway via interference of the CXXC5-Dvl interaction, significantly improved the overall pathogenic phenotypes of 5xFAD mice. Collectively, our findings revealed that CXXC5 plays a key role in AD pathogenesis and suggest inhibition of CXXC5-Dvl interaction as a new therapeutic approach for AD.

## 1. Introduction

Alzheimer's disease (AD) is the most prevalent neurodegenerative disease and is accompanied by cognitive dysfunction [1]. Accounting for nearly 70% of all dementia cases, AD is becoming a worldwide problem related to aging and genetic mutations, thereby causing massive burden on public health and society [2,3]. Therefore, therapeutic agents for the treatment of AD are urgently needed.

AD is characterized by two hallmark lesions: accumulation of pathological extracellular amyloid beta (Aβ) plaques and intracellular neurofibrillary tangles (NFT) formed by hyper-phosphorylated tau [4]. For decades, the amyloid hypothesis, which is based on the identification of neuropathological evidence related to Aβ aggregates and gene mutations that cause familial AD, has been the leading hypothesis for AD drug discovery [5–7]. However, owing to the complex pathogenesis of AD, numerous clinical trials of agents exclusively targeting Aβ to treat

*Abbreviations:* Aβ, amyloid beta; AD, Alzheimer's disease; ADAM10, a disintegrin and metalloproteinase 10; APP, amyloid precursor protein; BACE1, β-site APP cleaving enzyme 1; BBB, blood-brain barrier; CFC, contextual fear-conditioning; Ct, cycle threshold; CXXC5, CXXC finger protein 5; DAPI, 4′,6-diamidino-2-phenylindole; DKK1, dickopf-1; DKK3, dickopf-3; Dvl, dishevelled; ELISA, enzyme-linked immunosorbent assay; FDR, false discovery rate; GEO, Gene Expression Omnibus; GFAP, glial fibrillary acidic protein; GLP-1, glucagon-like peptide-1; GSK3β, glycogen synthase kinase 3β; Iba-1, ionized calcium-binding adaptor molecule-1; IHC, immunohistochemistry; Il-6, interleukin- 6; Il-1β, interleukin-1β; KY19334, 5-methoxyindirubin-3'-oxime; MsigDB, Molecular Signature Database; MWM, Morris water maze; NFT, neurofibrillary tangles; NEUROD1, neurogenic differentiation 1; NEUROG1, neurogenin 1; PAMPA, parallel artificial permeability membrane assay; PBS, phosphate buffered saline; PFA, paraformaldehyde; PSD95, postsynaptic density protein 95; PSEN1, presenilin-1; qPCR, quantitative PCR; SDS, sodium dodecyl sulfate; Th S, thioflavin S; Tnfα, tumor necrosis factor-α; WISP1, WNT1-inducible signaling pathway protein 1; WT, wild type.

* Corresponding author.
** Corresponding author at: Department of Biotechnology, College of Life Science and Biotechnology, Yonsei University, Seoul 03722, Republic of Korea.
*E-mail addresses:* y.kim@yonsei.ac.kr (Y. Kim), kychoi@ckregeon.com (K.-Y. Choi).

https://doi.org/10.1016/j.phrs.2023.106836
Received 28 February 2023; Received in revised form 20 June 2023; Accepted 21 June 2023
Available online 22 June 2023
1043-6618/© 2023 The Author(s). Published by Elsevier Ltd. This is an open access article under the CC BY-NC-ND license (http://creativecommons.org/licenses/by-nc-nd/4.0/).

AD have been unsuccessful [8]. Therefore, the present paradigm for the development of drugs for the treatment of AD has shifted to identifying new targets that mediate multiple pathogenesis of AD [9].

In recent years, number of studies have shown that the Wnt/β-catenin signaling pathway contributes to the pathogenesis of neurodegenerative diseases [6,10,11]. In particular, growing evidence suggests that dysregulation of the Wnt/β-catenin pathway is involved in multiple processes related to AD pathogenesis such as aging, synapse formation, neurogenesis, neuronal inflammation, and metabolism [12–14]. This wide range of involvement is related to the multiple target genes of the Wnt/β-catenin pathway associated with the pathology of AD including WNT1-inducible signaling pathway protein 1 (*WISP1*), glucagon-like peptide-1 (*GLP-1*), neurogenic differentiation 1 (*NEUROD1*), neurogenin 1 (*NEUROG1*), and a disintegrin and metalloproteinase 10 (*ADAM10*) [15–19]. In addition, activation of the Wnt/β-catenin pathway recovered cognitive function in AD model mice, and inhibited pathological processing of amyloid precursor protein (APP) by suppressing transcription of β-site APP cleaving enzyme 1 (*Bace1*) [20,21]. Furthermore, inhibition of glycogen synthase kinase 3β (GSK3β), which is a serine/threonine kinase known to hyperphosphorylate tau, resulted in the reduction of pathogenic features in AD model mice [22,23]. Moreover, analogs of Wnt/β-catenin target GLP-1 and its receptor agonists have been used for the development of drugs for AD [24,25]. However, the underlying molecular mechanisms and factors controlling Wnt/β-catenin pathway especially related with the AD pathogenesis are still poorly understood.

In this study, we discovered that the CXXC finger protein 5 (CXXC5), a negative regulator of the Wnt/β-catenin pathway which functions via direct interaction with the upstream component Dishevelled (Dvl) [26], plays major role in AD pathogenesis by suppressing the Wnt/β-catenin pathway.

## 2. Materials and methods

### 2.1. Human samples

Human hippocampus slides ($n = 5$) were purchased from Gold-Pacific (Seoul, Korea). Human prefrontal cortex slides ($n = 5$) were obtained from the Seoul National University Hospital (SNUH) Brain Bank. All samples derived from the SNUH Brain Bank were obtained with informed consent following the institutional review board-approved protocols (Approved IRB number: 1808–087–966). Detailed information on the human specimens is provided in the Supplementary Tables 1 and 2. Experiments involving human samples has been carried out in accordance with The Code of Ethics of the World Medical Association (Declaration of Helsinki), while all terms of Good Clinical Practice were applied.

### 2.2. Animal models

5xFAD (B6SJL-Tg (APPSwFlLon,PSEN1 *M146L*L286V)6799Vas/Mmjax) mice were purchased from Jackson Laboratory and maintained by mating with C57BL/6. SJL wild type (WT) mice. The generation of *Cxxc5*-/- mice has been previously described [26]. WT, 5xFAD, and *Cxxc5*$^{-/-}$/5xFAD mice littermates were obtained by intercrossing two lines for four generations and maintained on C57BL/6. SJL background. For comparative *Cxxc5*$^{-/-}$/5xFAD mice analyses, 9.5-month-old male WT, 5xFAD, and *Cxxc5*$^{-/-}$/5xFAD littermates were subjected to behavioral tests. Brain tissues were harvested and evaluated by immunohistochemistry (IHC) analyses. For age-dependent analyses for *Cxxc5*$^{-/-}$/5xFAD mice, 4-, 8-, and 12-month-old male WT, 5xFAD, and *Cxxc5*$^{-/-}$/5xFAD littermates were sacrificed and their brain tissues were subjected to IHC analyses. To determine the therapeutic potential of KY19334 (5-methoxyindirubin-3'-oxime) in 5xFAD mice, 11-month-old male 5xFAD mice were orally administered with KY19334 (25 mg/kg) or its vehicle [27] for 1 month, and their behavioral performance was compared with age-matched male WT mice administered with vehicle. Then, their brain tissues and other organs were harvested and evaluated by IHC analyses. For toxicity and side effect test of KY19334, 7-week-old male WT mice were purchased from Orient Bio Co. (Gyeonggi-do, Korea). WT mice were orally administered KY19334 (25 mg/kg) or vehicle for 2 months, and their phenotypes such as weight were consistently monitored. Brain and other organs were harvested and confirmed by histochemical analyses. All animals were maintained in a laboratory animal breeding room at Yonsei University under a 12 h light/12 h darkness cycle at 22–25 °C under conventional conditions and fed standard rodent chow diet and water. Prior to all animal experiments, the genotype of all mice were confirmed by PCR analyses of tail DNA using standard PCR conditions. All procedures were reviewed and approved by the ethical standards of Institutional Animal Care and Use Committee (IACUC) of Yonsei Laboratory Animal Research Center (IACUC-202101–1205–03, IACUC-202203–1426–01, and IACUC-202208–1524–01).

### 2.3. Learning and memory behavioral studies

To monitor cognitive function, we performed the Y-maze, contextual fear-conditioning (CFC), and Morris water maze (MWM) tests [28,29]. We used a three-arm horizontal maze (40 cm long and 10 cm wide with 12 cm high walls) for the Y-maze test, and the arms were symmetrically disposed at 120° angles from each other. Mice were placed at the end of a random arm allowing them to move freely through the maze during a 10-min session, and the number of total arm choices and sequence of arm choices were recorded. The percent alternation was defined by the proportion of arm choices that differ from the last two choices. Before each trial, the interior of the maze was cleaned with 70% ethanol to erase any irrelevant scents. The CFC test was performed as previously described [30]. On the first day, the mice were placed into a cued box for 5 min for habituation and exploration. The next day, for training, mice were placed into a sound-attenuating standard operant chamber (Coulbourn, PA) for 3 min. A 30 s tone (3 kHz, 85 dB) was delivered followed by a 1 s foot shock (0.5 mA). This training was repeated twice continuously within a 90 s interval. One day later, for contextual retention tests, mice were subjected to the same conditioning chamber and the freezing response was measured for 5 min. Responses were recorded using a video camera to score freezing. For the MWM test [31], a circular water tank (120 cm diameter, 25 ± 1 °C) with hidden quadrants was used. A 12 cm (diameter) escape platform was placed 1.5 cm below the water surface. The quadrant containing the platform refers to the target zone. The hidden platform test was performed for 6 days. The mice were trained for 6 consecutive days with five trials per day as acquisition trials. Each trial began by placing the mice into a different quadrant and allowing them to swim freely for 60 s. After each mouse reached or was guided to the platform, they were returned to their home cage and dried for 20 min. The time taken by each mouse to reach the platform refers to the escape latency. On the seventh day, a probe test was performed for 60 s to determine memory retention without the platform. Each mouse was placed into the opposite quadrant of the target zone where the platform was removed (time in the target zone). The numbers of crossings in the probe were also calculated. Data were recorded and analyzed using a video camera-based Ethovision System (Nodulus, Netherlands). All recordings of behavioral responses were transcribed manually into the computer-acceptable format while keeping the experimenter blind.

### 2.4. Immunohistochemistry analyses

After each animal study, mice were anaesthetized by intraperitoneal injection of 2% avertin (20 μg/g) and perfused with 0.9% saline followed by ice-cold 4% paraformaldehyde (PFA). Excised brains were post-fixed overnight in 4% PFA at 4 °C, immersed in 30% sucrose for 48 h, and embedded in optimal cutting temperature compound (Leica

biosystems company, Wetzlar, Germany). The hippocampal tissues were sectioned (35 μm; average range) using Cryostat (Microm HM 525, Thermo Scientific, MA) and mounted onto glass slides. The sections were air-dried for 30 min at room temperature and incubated in phosphate buffered saline (PBS, pH 7.4) for 5 min. For antigen retrieval, the slides were incubated in 1% (w/v) sodium dodecyl sulfate (SDS) in PBS for 10 min and blocked with 20% (v/v) horse serum in PBS for 1 h at room temperature. The sections were incubated overnight at 4 °C with primary antibodies against β-catenin (1:100; BD Transduction Laboratories, KY), CXXC5 (1:100; lab-made), 6E10 (1:100; Covance, NC), glial fibrillary acidic protein (GFAP; 1:200; Millipore, MA), ionized calcium-binding adaptor molecule-1 (Iba-1; 1:100; Millipore), gliotransmitter γ-aminobutyric acid (GABA; 1:100; Millipore), or postsynaptic density protein 95 (PSD95; 1:100; NeuroMab, CA). The tissue sections were washed with PBS, incubated with Alexa Fluor 488- (Invitrogen, Carlsbad, CA), Alexa Fluor 555- (Invitrogen), or Alexa Fluor 647- (Abcam, Cambridge, UK) conjugated IgG secondary antibody (1:200) at room temperature for 1 h and counterstained with 4′,6-diamidino-2-phenylindole (DAPI; 1:3000; Boehringer Mannheim, Baden-Wurttemberg, Germany). Aβ plaques in the brain were visualized using thioflavin S (Th S) staining. Th S was dissolved in 50% of ethanol at 500 μM and the brain sections were stained for 7 min. To remove nonspecific binding of the dye, the sections were washed with 100%, 90%, and 70% ethanol solutions for 1 min each and then washed with PBS. Fluorescent signals were detected using an LSM700 META (Carl Zeiss, Gottingen, Germany) confocal microscopy.

### 2.5. RNA extraction and quantitative PCR

Total RNA was extracted from the ground tissue powder using TRIzol reagent (Invitrogen) according to the manufacturer's instructions. Reverse transcription was performed using M-MLV reverse transcriptase (Invitrogen) and 2 μg of total RNA. Synthesized cDNA was diluted to a concentration of 100 ng/μl, and quantitative PCR (qPCR) analyses were performed using a Rotor-gene Q real-time PCR cycler (Qiagen, Hilden, Germany) using SYBR green reagent (Qiagen). The conditions were: 95 °C for 10 min followed by 40 cycles at 95 °C for 5 s, and 60 °C for 15 s. The relative mRNA levels were quantified using the comparative cycle threshold (Ct) method (ΔΔCt). All mRNA levels were normalized to those of *GAPDH*. Primer sequences are listed in Supplementary Table 3.

### 2.6. Immunoblotting analyses

Tissues were ground and lysed in RIPA buffer (150 mM NaCl, 10 mM Tris, pH 7.2, 0.1% SDS, 1.0% Triton X-100, 1% sodium deoxycholate, and 5 mM EDTA). Samples were separated on 10–12% SDS polyacrylamide gels and transferred onto PROTRAN nitrocellulose membranes (Schleicher and Schuell Co, NY). After blocking with PBS containing 5% non-fat dry skim milk and 0.07% (vol/vol) Tween 20, membranes were incubated with antibodies against β-catenin (1:1000; Santa Cruz Biotechnology, Inc., TX), CXXC5 (1:1000; lab-made), BACE1 (1:1000, Abcam), GFAP (1: 1000; Millipore), Iba-1 (1: 1000; Millipore), p-GSK3β (S9) (1:1000; Cell Signaling Technology, MA), APP (1:1000; Abcam), or Erk (1:5000; Cell Signaling Technology) at 4 °C overnight. Samples were then incubated with horseradish peroxidase–conjugated anti-rabbit (1:5000; Bio-Rad Laboratories, CA) or anti-mouse IgG secondary antibody (1:5, 000; Cell Signaling Technology). Protein bands were visualized using an enhanced chemiluminescence kit (Amersham Bioscience, Piscataway, NJ) and a luminescent image analyzer, LAS-4000 (Fujifilm, Tokyo, Japan).

### 2.7. Human-Aβ ELISA and PAMPA-BBB assay

A guanidine buffer (5 mM guanidine-HCl, 50 mM Tris-HCl pH 8.0) containing 1 × proteinase inhibitor cocktail was added to the pellet of brain lysates. The mixtures were then incubated at room temperature for 3 h with shaking to dissolve the Aβ-insoluble fraction. After centrifugation at 4 °C for 2 h, the levels of dissolved Aβ in the supernatant were measured using a Human Aβ 1–42 sandwich enzyme-linked immunosorbent assay (ELISA) kit (Invitrogen). Protein concentrations of the insoluble fractions were normalized using the Bradford protein assay, and subsequent measurements were performed according to the manufacturer's instructions. The blood-brain barrier (BBB) permeability of KY19334 was tested by using BBB-parallel artificial permeability membrane assay (PAMPA) kit (Pion, Inc., MA) according to the manufacturer's instructions.

### 2.8. Bioinformatics data analyses

Molecular pathway dysregulation in the human hippocampal tissues was determined by gene set enrichment analyses, surveying the molecular pathway gene set in the Molecular Signature Database (MsigDB) (www.broadinstitute.org/msigdb). Cross-species comparison of transcriptomic dysregulation was performed in the space of molecular pathway gene sets from KEGG databases, and statistically significant dysregulation was defined as a false discovery rate (FDR) $< 0.01$ in either of the two human hippocampus CA1 tissue transcriptome datasets: normal ($n = 8$) vs. AD ($n = 7$) patients (GSE28146).

### 2.9. Statistical analyses

Statistical analyses were performed using unpaired two-tailed Student's t-test. Asterisks indicate statistically significant differences (*, $P < 0.05$; **, $P < 0.005$; ***, $P < 0.0005$). Information regarding the statistical details and methods is indicated in the figure legends, tests, or methods.

## 3. Results and discussion

### 3.1. CXXC5 is induced in the brain tissues of AD patients

To identify the role of CXXC5 in AD development, we used gene set enrichment analyses to investigate the mRNA expression profiles of CXXC5 and Wnt-responsive genes in AD patients (Gene Expression Omnibus [GEO]: GSE28146). The microarray analyses results showed that the mRNA levels of the Wnt/β-catenin pathway target genes such as *AXIN2*, *TCF7L2*, *WISP1,* and *GLP-1* were lower in the hippocampus CA1 tissues from AD patients compared to those of paired normal tissues (Fig. 1A, B). However, the mRNA level of *CXXC5*, a negative regulator of the Wnt/β-catenin pathway, and inhibitors of Wnt/β-catenin pathway such as dickopf-1 (*DKK1*), dickopf-3 (*DKK3*), and *GSK3β* were higher in the hippocampus CA1 tissues of AD patients compared to those of normal individuals (Fig. 1B). To confirm the level of CXXC5 in AD brain tissue, we analyzed the hippocampus and prefrontal cortex tissues of normal individuals and AD patients using IHC analyses (Supplementary Tables 1 and 2). Th S, which visualizes dense-core Aβ plaques [32], was used to distinguish AD tissues from normal tissues. The protein level of CXXC5 was highly upregulated and mostly localized in the cytosol of hippocampal cells, whereas the level of β-catenin was lowered in the AD patient hippocampus tissues compared with those of normal individuals (Fig. 1C, D and Fig. S1A). Similarly, the levels of CXXC5 and β-catenin were inversely correlated in the prefrontal cortex tissues of AD patients (Fig. S1B-D). We further compared the expression level of CXXC5 with other representative disease markers in hippocampus of AD patients by IHC analyses. We monitored 6E10 and Th S markers to confirm dense core and diffuse plaques [33], GFAP and GABA to confirm reactive astrocytes and inflammation [34], Iba-1 to confirm microgliosis [30], and PSD95 to confirm the structural and functional integrity of synapses [35]. As is known, we confirmed that the levels of 6E10, Th S, GFAP, GABA, and Iba-1 were upregulated, and the levels of PSD95 were decreased in the hippocampus tissues of AD patients compared to that of normal individuals (Fig. 1E, F). We identified that the levels of 6E10, Th

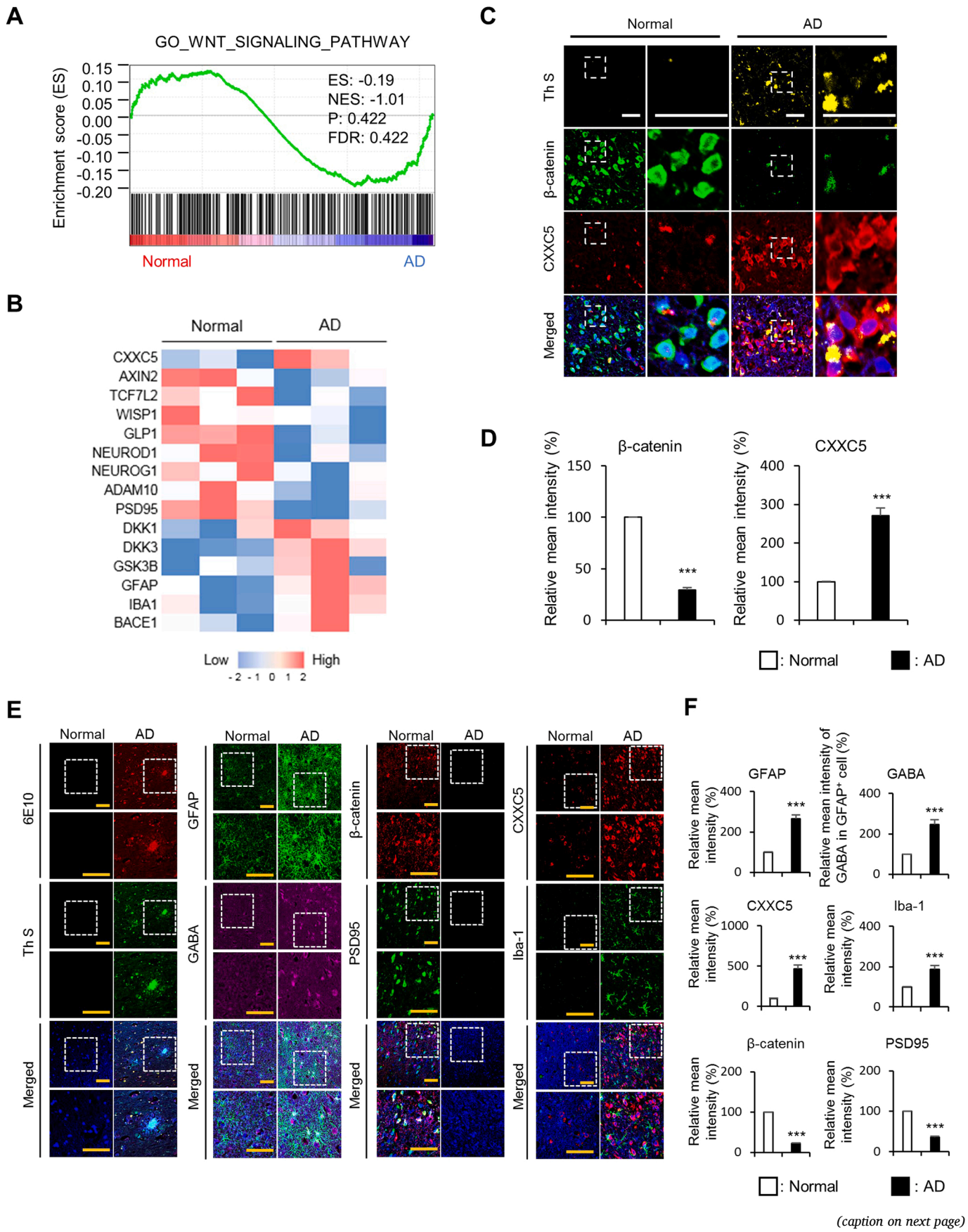


*(caption on next page)*

**Fig. 1.** CXXC5 was induced in hippocampus of AD patients. (A) Gene set enrichment analyses of microarray transcriptome data for normal and hippocampus CA1 tissues of AD patients for Wnt/β-catenin signaling-activated gene signature. Black columns indicate 293 enriched genes involving the Wnt/β-catenin signaling pathway (normal, $n = 8$; AD, $n = 7$). ES, enrichment score; NES, normalized enrichment score; FDR, false discovery rate; P, probability value. (B) Hierarchical clustering and heat-map of RNA-seq data in the hippocampus CA1 tissues from normal individuals ($n = 3$) and AD patients ($n = 3$). The color scale shows Z-score fragments per kilobase of transcript per million mapped reads representing the mRNA levels of each gene in the blue (low expression) to red (high expression) colored scheme. (C) Representative images for IHC analyses of Th S, β-catenin and CXXC5 in human hippocampus. White scale bars, 50 μm. (D) Relative mean intensity values of β-catenin and CXXC5 shown in Fig. 1C ($n = 5$, independent experiments). (E) Representative images for IHC analyses of 6E10, Th S, GFAP, GABA, CXXC5, Iba-1, β-catenin, and PSD95 in human hippocampus. Yellow scale bars, 100 μm. (F) Relative mean intensity values for Fig. 1E ($n = 5$, independent experiments). Values are expressed as means ± SEM. * , $P < 0.05$; * *, $P < 0.005$; * ** , $P < 0.0005$, significantly different from normal.

S, GFAP, GABA, and Iba-1 were positively correlated, and the levels of β-catenin and PSD95 were negatively correlated with the level of CXXC5 in the AD patient's hippocampus tissues (Fig. 1E, F). In summary, overexpressed CXXC5 suppresses the Wnt/β-catenin pathway and is a causative factor of AD.

### 3.2. *Cxxc5 is upregulated in brain tissues of 5xFAD mice*

To confirm the role of Cxxc5 in mouse model of AD, we analyzed 5xFAD transgenic mice that overexpressed *App* and presenilin-1 (*Psen1*) containing five familial AD mutations [36]. As the AD patients, we found that Cxxc5 was overexpressed and mainly localized in the cytosol of hippocampal cells with suppression of β-catenin in the hippocampus CA1 regions of 5xFAD mice compared with that of WT mice (Fig. 2A, B). We also found that the level of Cxxc5 was similarly upregulated throughout the prefrontal cortex and other hippocampus regions (DG, CA2, and CA3) in 5xFAD mice (Fig. S2A). We further examined the level of Cxxc5 in 5xFAD and WT mouse brain tissues using immunoblot analyses to further confirm the relationship between Cxxc5, Wnt/β-catenin pathway, and AD markers. The protein levels of Cxxc5 were upregulated and positively correlated with those of GFAP, Iba-1, and BACE1, whereas the Wnt/β-catenin pathway was suppressed as shown by the decrease in of the levels of β-catenin, GSK-3β (S9), an inactive form of GSK-3β, and ADAM10 (Fig. 2C, D). Furthermore, we investigated the relationship between Cxxc5 and other representative AD markers in the hippocampal cells of 5xFAD mice using IHC analyses. The protein levels of Cxxc5 were significantly upregulated with increment of 6E10, Th S, GFAP, GABA, and Iba-1, and were negatively correlated with levels of β-catenin and PSD95 (Fig. 2E, F). We also found similar expression patterns of identical markers in the prefrontal cortex and other hippocampus regions (DG, CA2, and CA3) of 5xFAD mice (Fig. S2B-E). Overall, Cxxc5 overexpression was correlated with 5xFAD mice pathogenesis.

### 3.3. *Cxxc5 level increases in 5xFAD mice brain in age-dependent manner*

5xFAD mice exhibit robust pathological phenotypes with increasing age including plaque deposition, neuronal inflammation, and microgliosis [28,37]. To profile the expression patterns of Cxxc5 with other AD-related markers in an age-dependent manner, we examined age-matched male 4-, 8-, 12- month WT and 5xFAD mice brain tissues using IHC analyses [38]. We confirmed that the level of Cxxc5 gradually increased and was positively correlated with the levels of 6E10, Th S, GFAP, GABA and Iba-1, and inversely correlated with the levels of β-catenin and PSD95 in the hippocampus CA1 region of 5xFAD mice with aging (Fig. 3). Similar expression patterns of the identical markers were confirmed in age-dependent WT, 5xFAD mice prefrontal cortex and other hippocampus regions (DG, CA2, and CA3) (Fig. S3). These results show that the age-dependent increment of Cxxc5 may participate in the severity of 5xFAD mice pathological phenotypes related to aging.

### 3.4. *Ablation of Cxxc5 ameliorates AD phenotypes in 5xFAD mice*

To confirm the role of Cxxc5 in AD development in 5xFAD mice, we generated *Cxxc5*$^{-/-}$/5xFAD mice. We performed Y-maze, CFC, and MWM tests on 9.5-month-old WT ($n = 5$), 5xFAD ($n = 5$), and *Cxxc5*$^{-/-}$/5xFAD ($n = 5$) mice to monitor cognitive function (Fig. 4A). Cognitive capability was determined with the percent alternation in the Y-maze. We found that ablation of *Cxxc5* rescued behavioral performance in the Y-maze test in *Cxxc5*$^{-/-}$/5xFAD mice compared to age-matched 5xFAD mice (Fig. 4B). However, the total number of individual arm entries did not differ significantly, as shown in the Y-maze test (Fig. 4C). Next, the emotion-associated learning capability based on amygdala-hippocampal communication was analyzed by using the CFC tests, measuring the freezing response [39]. The performance of *Cxxc5*$^{-/-}$/5xFAD mice in the CFC tasks was mostly rescued as a level of WT (Fig. 4D). Finally, in the MWM task, *Cxxc5*$^{-/-}$/5xFAD mice also showed significantly improved behavioral performance compared with age-matched 5xFAD mice (Fig. 4E-I). Th S and 6E10 staining of the hippocampus tissues from the identical mice of behavioral tests showed that the number and area of plagues were significantly rescued in *Cxxc5*$^{-/-}$/5xFAD mice compared to 5xFAD mice (Fig. 4J, K). To analyze the change in the level of insoluble Aβ in the hippocampus by *Cxxc5* ablation, we performed human Aβ ELISA. We confirmed that the level of insoluble Aβ, which was increased in 5xFAD mice, was returned to the level in WT mice in the hippocampus of *Cxxc5*$^{-/-}$/5xFAD mice (Fig. 4L). Collectively, these results show that ablation of *Cxxc5* improves cognitive capability with reduction of Aβ plagues in 5xFAD mice.

To correlate behavioral improvement with the molecular signature of AD in the *Cxxc5*$^{-/-}$/5xFAD mice, the mice used for the aforementioned behavioral tests were subjected to histochemical analyses. The protein levels of GFAP, GABA, and Iba-1 were dramatically reduced in the hippocampus CA1 region of *Cxxc5*$^{-/-}$/5xFAD mice compared to those of 5xFAD mice, and were almost equivalent to those of WT mice (Fig. 4M, N). In contrast, the protein levels of both β-catenin and PSD95 in *Cxxc5*$^{-/-}$/5xFAD mice were recovered to levels similar to those in the WT mice (Fig. 4M, N). Similarly, these expression patterns of AD-related markers were also observed in prefrontal cortex and other hippocampus region (DG, CA2, and CA3) of *Cxxc5*$^{-/-}$/5xFAD mice (Fig. S4). The levels of the Wnt/β-catenin pathway target genes which are related to AD and are suppressed in 5xFAD mice such as *Axin, Tcf7l2, Wisp1, Glp1, Neurod1, Neurog1, Adam10*, and *Dlg4* were also restored in *Cxxc5*$^{-/-}$/5xFAD mice as the levels of WT mice (Fig. 4O). In contrast, the mRNA levels of *Bace1, Gfap, Aif1*, and neuronal inflammation-related genes such as tumor necrosis factor-α (*Tnfα*), interleukin-1β (*Il-1β*), and interleukin- 6 (*Il-6*), which were increased in 5xFAD mice, were reduced in *Cxxc5*$^{-/-}$/5xFAD mice at the level of WT mice (Fig. 4O, P). The immunoblot analyses showed that the protein levels of β-catenin, p-GSK3β (S9), GFAP, Iba-1, BACE1, and ADAM10 in *Cxxc5*$^{-/-}$/5xFAD mice were recovered to levels similar to those in the WT mice (Fig. 4Q). To confirm the consequence of *Cxxc5* ablation in age-dependent expression patterns of AD-related markers, we analyzed age-matched hippocampus CA1 tissues of the 4, 8, 12 month WT, 5xFAD and *Cxxc5*$^{-/-}$/5xFAD mice using IHC analyses (Fig. S5). We confirmed that the levels of 6E10, Th S, GFAP, GABA, Iba-1, β-catenin, and PSD95 in 4, 8, 12 month *Cxxc5*$^{-/-}$/5xFAD mice were recovered as the levels similar to WT mice (Fig. S5). These results demonstrate that targeting CXXC5 is a potential approach for the development of therapeutic agents for treating AD.

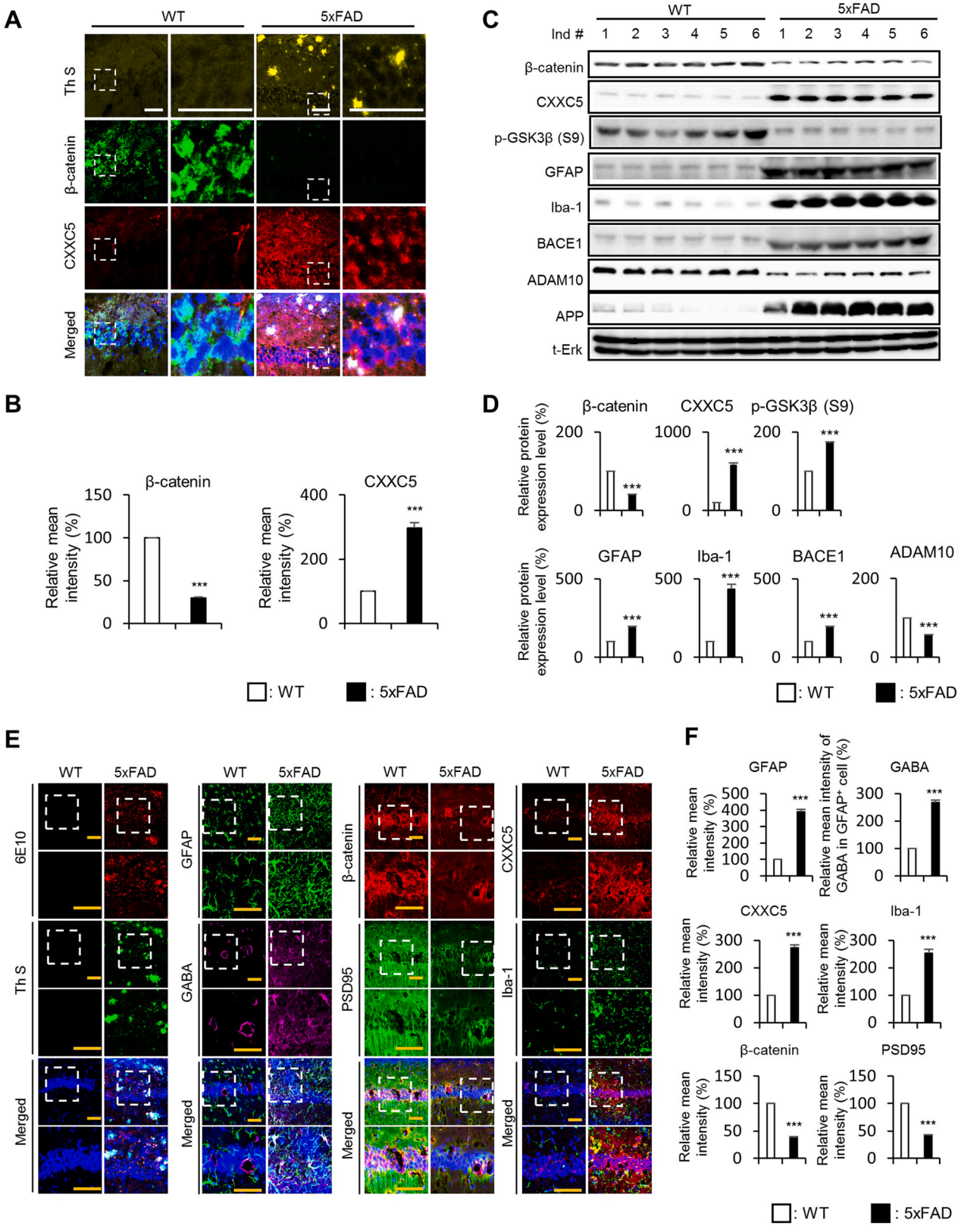


**Fig. 2.** Cxxc5 was induced in hippocampus of 5xFAD mice. (A-F) Ten-month-old male WT and 5xFAD mice were sacrificed and subjected to brain analyses. (A) Representative images for IHC analyses of Th S, β-catenin and Cxxc5 in hippocampus CA1 tissues. White scale bars, 50 μm. (B) Relative mean intensity values of β-catenin and Cxxc5 shown in Fig. 2A ($n = 3$, independent experiments) (C) Immunoblotting analyses data. (D) Quantification of the intensities of protein images shown in Fig. 2C ($n = 6$, independent mice). (E) Representative images for IHC analyses of 6E10, Th S, GFAP, GABA, Cxxc5, Iba-1, β-catenin, and PSD95 in hippocampus CA1 tissues. Yellow scale bars, 100 μm. (F) Relative mean intensity values of β-catenin, PSD95, Cxxc5, Iba-1, GFAP, and GABA shown in Fig. 2E ($n = 3$, independent experiments). Values are expressed as means ± SEM. * , $P < 0.05$; * *, $P < 0.005$; * ** , $P < 0.0005$, significantly different from WT.

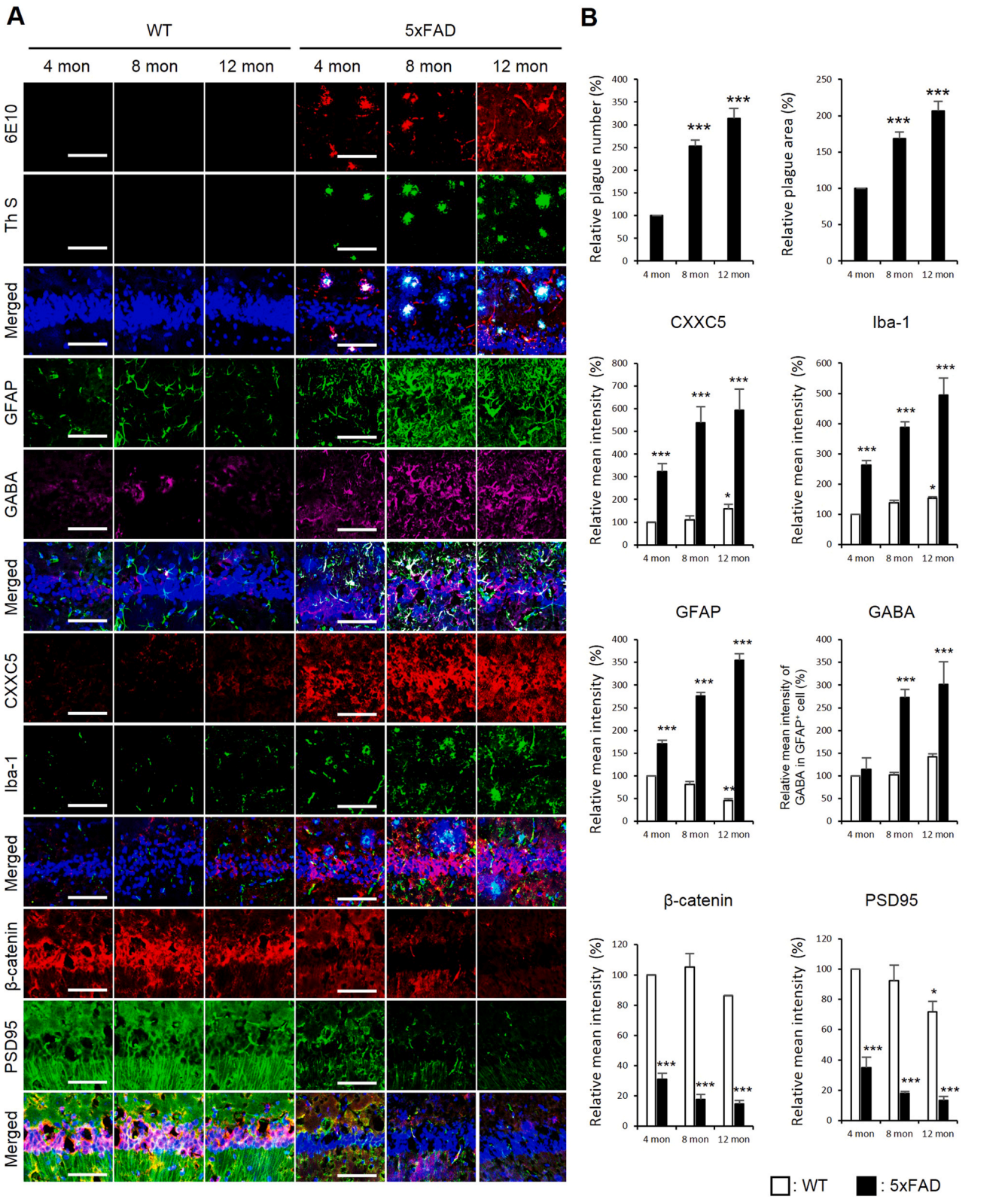


**Fig. 3.** Age-dependent expression of Cxxc5 and AD markers in 5xFAD mice hippocampus CA1. (A, B) Brains of male WT and 5xFAD mice at 4-, 8-, 12-month time-point were sliced and subjected to IHC analyses as described in Materials and Methods. (A) Representative image for IHC analyses of 6E10, Th S, GFAP, GABA, Cxxc5, Iba-1, β-catenin, and PSD95 in hippocampus CA1 tissues. Scale bars, 100 μm. (B) Relative number and area of plaques, and mean intensity values of the protein intensities shown in Fig. 3A ($n = 3$, independent experiments). Number or area of plaques are normalized (%) to the level of the 4 month 5xFAD mice, and mean intensity values are normalized to the levels of 4 month WT mice. Values are expressed as means ± SEM. * , $P < 0.05$; * *, $P < 0.005$; * ** , $P < 0.0005$, significantly different from 4 month 5xFAD or 4 month WT mice.

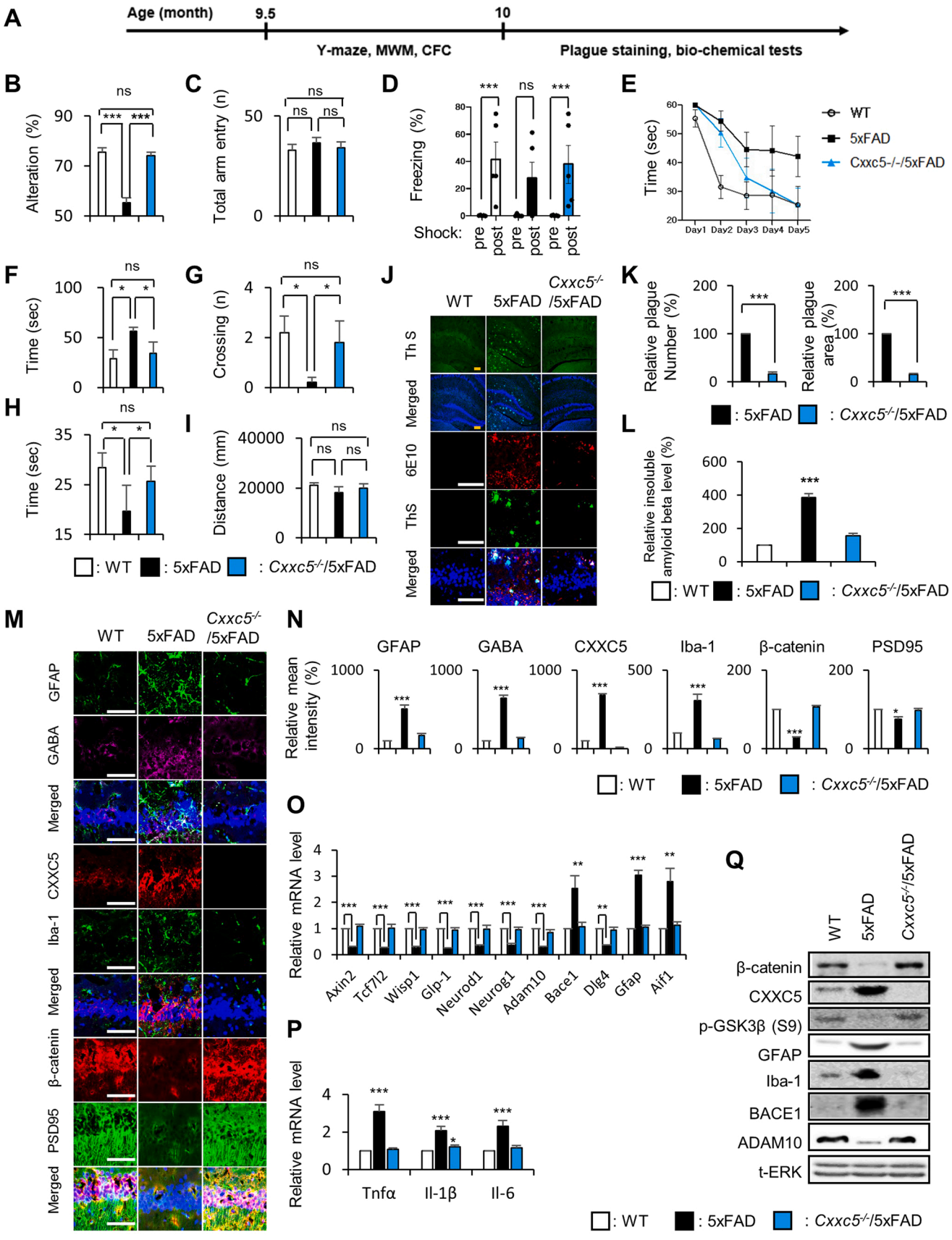


*(caption on next page)*

**Fig. 4.** Deletion of *Cxxc5* rescues AD phenotype by restoring Wnt/β-catenin signaling in 5xFAD mice. (A-I) Y-maze, fear-conditioning and Morris water maze tests on 9.5-month-old male WT ($n = 5$), 5xFAD ($n = 5$), *Cxxc5*$^{-/-}$/5xFAD ($n = 5$) mice. (J-Q) Mouse used for behavioral tests were sacrificed and subjected to brain analyses. (A) A schematic presentation for the time course for experiments. (B) Relative percent alternations in the Y-maze tests. (C) Total entry numbers into each arm in the Y-maze tests. (D) Relative percent of total freezing from contextual fear conditioning tests. (E) Escape latency of the training days in the Morris water maze. (F) Escape latency of probe test in the Morris water maze. (G) Number of platform crossings during probe test in the Morris water maze. (H) Time spent in the target quadrant during a 60 s probe test in the Morris water maze. (I) Total distance travelled during the probe test in the Morris water maze. (J) Representative images for IHC analyses of Th S in the hippocampal region (yellow scale bars, 200 μm), and 6E10, Th S co-staining in the hippocampus CA1 (white scale bars, 100 μm). (K) Relative number and area of the plaques shown in Fig. 4J ($n = 3$, independent experiments). (L) Sandwich ELISA of Aβ-insoluble fractions in hippocampal lysates. (M) Representative images for IHC analyses of GFAP, GABA, Cxxc5, Iba-1, β-catenin, and PSD95 in hippocampus CA1 tissues. Scale bars, 100 μm. (N) Relative mean intensity values of Fig. 4M ($n = 3$, independent experiments). (O) Relative mRNA expression of Wnt/β-catenin pathway target genes and AD related genes. (P) Relative mRNA expression of neuronal inflammation related genes. (Q) Immunoblotting analyses data for hippocampal lysates. Number or area of plaques are normalized (%) to the levels of 5xFAD. Values are expressed as means ± SEM. * , $P < 0.05$; * *, $P < 0.005$; * ** , $P < 0.0005$, significantly different from WT or 5xFAD.

### *3.5. KY19334 attenuates the pathological features of AD in 5xFAD mice by restoring the suppressed Wnt/β-catenin pathway*

As an approach to inhibit CXXC5 function and investigate its effects on the pathological phenotypes of AD, we adapted KY19334, an indirubin derivative small molecule that activates the Wnt/β-catenin pathway by blockade of CXXC5 function through interference of its interaction with Dvl [40]. The KY19334 penetrates the BBB as revealed by parallel artificial PAMPA in vitro (Fig. S6) and provides an advantage for optimal activation of the Wnt/β-catenin pathway by its known role as a GSK3β inhibitor [40,41]. To test the effect of KY19334 in vivo, we orally administered KY19334 at 25 mpk in 11-month-old male 5xFAD mice ($n = 10$) for a month, and their behavioral changes were compared with those of age-matched 5xFAD ($n = 8$) and WT mice ($n = 10$) (Fig. 5A). Administration of KY19334 significantly recovered behavioral performance defects in 5xFAD mice in the Y-maze without affecting total arm entry (Fig. 5B, C). The lowered performance of the 5xFAD mice shown in the CFC tasks was significantly recovered by the application of KY19334 (Fig. 5D). KY19334 treated 5xFAD mice also showed significant cognitive improvement as shown in the MWM task compared with that of age-matched vehicle treated 5xFAD mice (Fig. 5E-I). The number and area of plague were significantly reduced in KY19334 treated 5xFAD mice hippocampus as revealed by Th S and 6E10 staining (Fig. 5J, K). We also confirmed decrement of insoluble Aβ in KY19334 treated 5xFAD mice hippocampus tissue (Fig. 5L). Overall, these results show that restoration of Wnt/β-catenin pathway by blockade of CXXC5 function significantly rescues hippocampus-dependent-cognitive deficits and with reduction of Aβ plagues.

To confirm the mode of action of KY19334 in behavioral improvement in 5xFAD mice, the identical mice used for behavioral tests were subjected to histochemical analyses. The protein levels of GFAP, GABA, and Iba-1 which were increased in 5xFAD mice were significantly lowered by KY19334 treatment (Fig. 5M, N). In contrast, the protein levels of β-catenin and PSD95 were restored in the 5xFAD mice treated with KY19334 as the levels similar to WT mice in the hippocampus CA1 region (Fig. 5M, N). The reduction of AD-related markers and recovery of the Wnt/β-catenin pathway were also observed in the prefrontal cortex and other hippocampus regions (DG, CA2, and CA3) of KY19334-treated 5xFAD mice (Fig. S7). The mRNA levels of Wnt/β-catenin pathway target genes and AD-related genes (*Axin, Tcf7l2, Wisp1, Glp1, Neurod1, Neurog1, Adam10,* and *Dlg4*) were significantly increased by KY19334 treatment (Fig. 5O). In contrast, the levels of the pathology related genes for AD, *Bace1, Gfap,* and *Aif1* were reduced by KY19334 treatment (Fig. 5O). The mRNA levels of genes related to neuronal inflammation were also decreased by KY19334 treatment (Fig. 5P). The protein levels of β-catenin, p-GSK3β (S9), GFAP, Iba-1, BACE1, and ADAM10 in KY19334 treated 5xFAD mice were recovered to levels similar to those in WT mice as confirmed by immunoblot analyses (Fig. 5Q). The target for KY19334 is CXXC5-Dvl PPI, not the CXXC5 itself including its level change [40]. We confirmed the protein level of Cxxc5 were not significantly altered by KY19334 treatment (Fig. 5M, N, and Q).

The Wnt/β-catenin pathway is considered a promising target for drug development; however, the main issue targeting this pathway is safety, especially the potential outcome of cancer due to its aberrant activation [42]. We observed no significant changes in body weights and anomalies in apparent phenotypes and weight of organs after KY19334 treatment (Fig. S8). Moreover, we did not observe any oncogenic property by long-term breeding of *Cxxc5*$^{-/-}$ mice or any side-effects by long-term treatment of KY19334 to WT mice (Fig. S9). Our approach for restorative activation of the suppressed Wnt/β-catenin pathway by blockade of the negative regulatory factor CXXC5 at upstream provides a safe approach for the activation of the whole pathway. Overall, these results indicate that KY19334 effectively recovers AD phenotypes with safety in 5xFAD mice by restorative activating the Wnt/β-catenin pathway through blockade of the CXXC5 function.

## 4. Conclusion

AD is the most common neurodegenerative disorder associated with cognitive deficits, and is considered a vital threat to public health [6,43]. However, owing to the complexity of the pathophysiological features of AD, clinical trials of Aβ-targeting drugs for the treatment of AD have been unsuccessful [44–46]. Therefore, the AD drug discovery paradigm has shifted to identifying and targeting new factors that control the multiple pathophysiological processes of AD [6,9,47].

The Wnt/β-catenin pathway is one of the major signaling pathways involved in the regeneration of damaged tissues as well as the early development of animals [48]. Growing evidence suggests that the Wnt/β-catenin signaling pathway is a major subject for understanding the complexity of AD development [13,49]. However, the underlying molecular mechanisms and factors controlling the Wnt/β-catenin pathway, particularly those related to AD pathogenesis, remain unexplored.

In this study, we identified CXXC5 as a key factor causing AD. The CXXC5 is overexpressed in the hippocampus and prefrontal cortex of brain tissues of the AD patients and 5xFAD mice, with suppression of the Wnt/β-catenin pathway. The level of CXXC5 was positively correlated with AD-related markers such as 6E10, Th S, GFAP, GABA, and Iba-1, and negatively correlated with levels of β-catenin and PSD95 in AD patient and 5xFAD mice brain tissues. In addition, the age-dependent Cxxc5 increment especially prominent in 5xFAD mice paired with AD-related markers. The hypothesis that interference of CXXC5 function restoratively activate Wnt/β-catenin pathway by targeting the CXXC5-Dvl PPI as a novel target for AD drug development was further confirmed by absence of the AD pathological features in the *Cxxc5*$^{-/-}$/5xFAD mice and significant recovery of the pathological phenotypes in the KY19334-applied 5xFAD mice.

Taken together, these results indicate that CXXC5 plays role as a major driver for AD pathogenesis, and blockade of CXXC5 function via inhibition of the CXXC5-Dvl PPI is a potential therapeutic approach for the treatment of AD.

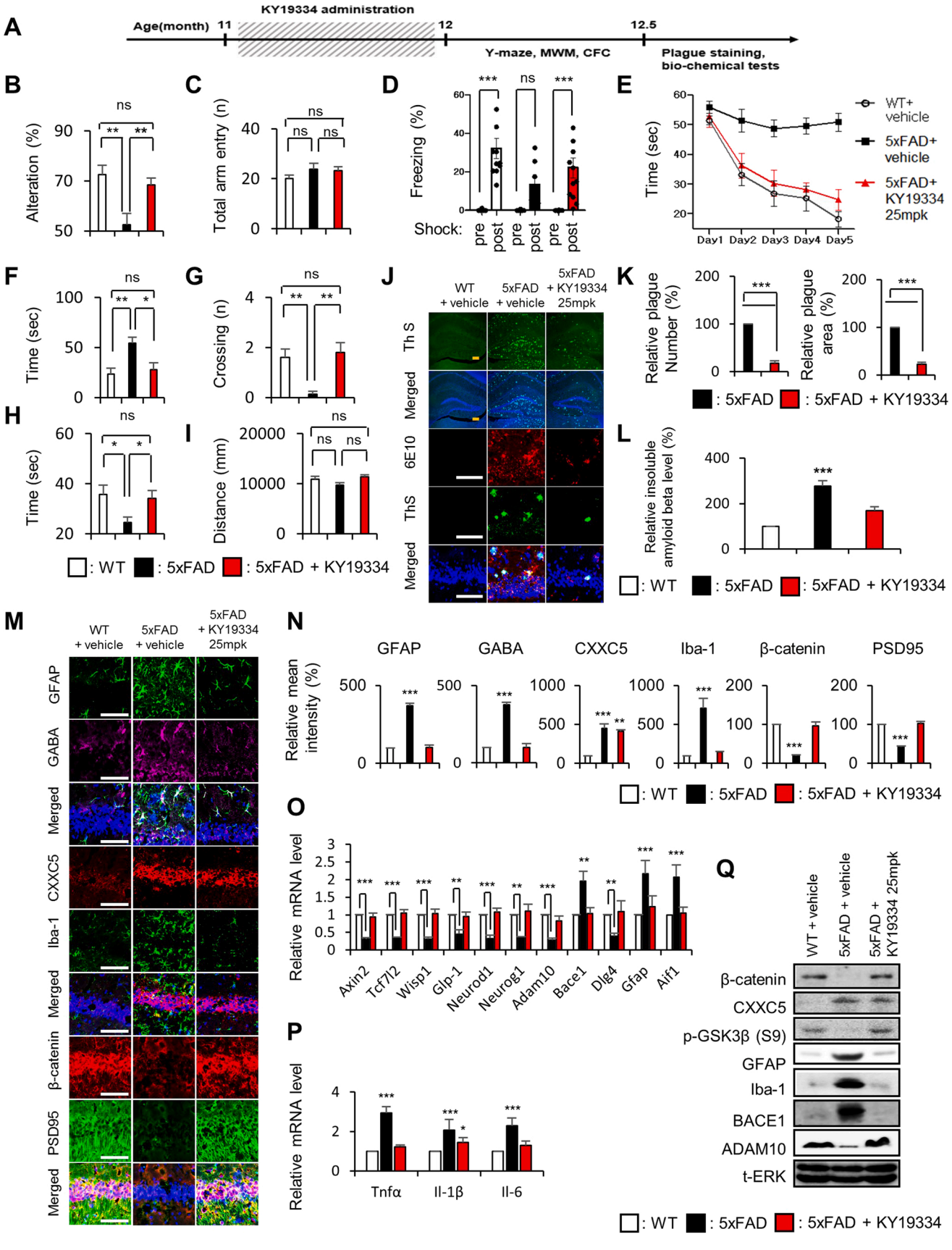


*(caption on next page)*

**Fig. 5.** Blockade of Cxxc5-Dvl interaction with KY19334 recovers multiple pathological phenotypes of the 5xFAD mice. (A-I) Eleven-month-old male 5xFAD mice were orally administered with vehicle ($n = 8$) or 25 mpk KY19334 ($n = 10$) for 1 month, and their behavioral changes were compared with age-matched those of male WT mice orally administered with vehicle ($n = 10$) using Y-maze, fear-conditioning and Morris water maze tests. (J-Q) The mice used for behavioral tests were sacrificed and subjected to brain analyses. (A) A schematic presentation for the time course for experiments. (B) Relative percent alternations of the Y-maze tests. (C) Total entry numbers into each arm in the Y-maze tests. (D) Relative percent of total freezing from contextual fear conditioning tests. (E) Escape latency of the training days in the Morris water maze. (F) Escape latency of probe tests in the Morris water maze. (G) Number of platform crossings during probe tests in the Morris water maze. (H) Time spent in the target quadrant during a 60 s probe tests in the Morris water maze. (I) Total distance travelled during the probe tests in the Morris water maze. (J) Representative images for IHC analyses of Th S in the hippocampal region (yellow scale bars, 200 μm), and 6E10, Th S co-staining in the hippocampus CA1 (white scale bars, 100 μm). (K) Relative number and area of the plaques shown in Fig. 5J ($n = 3$, independent experiments). (L) Sandwich ELISA of Aβ-insoluble fractions in hippocampal lysates. (M) Representative images for IHC analyses of GFAP, GABA, Cxxc5, Iba-1, β-catenin, and PSD95 in hippocampus CA1 tissues. Scale bars, 100 μm. (N) Relative mean intensity values of Fig. 5M ($n = 3$, independent experiments). (O) Relative mRNA expression of Wnt/β-catenin pathway target genes and AD related genes. (P) Relative mRNA expression of neuronal inflammation related genes. (Q) Immunoblotting analyses data of hippocampal lysates. Number or area of plaques are normalized (%) to the levels of 5xFAD. Values are expressed as means ± SEM. * , $P < 0.05$; * *, $P < 0.005$; * ** , $P < 0.0005$, significantly different from WT + vehicle or 5xFAD + vehicle.

## CRediT authorship contribution statement

M.Y., H.K., H.S., H.L., and M.-J.K. conducted experiments, and collected and analyzed data. M.Y., H.S., and H.L. conceptualized and designed experiments, discussed results, and interpreted data. S.-H.P. and G.H. provided resources. M.Y., Y.K., and K.-Y.C. designed figures and wrote the manuscript. M.Y. conducted revision experiments. M.Y and K.-Y.C revised the manuscript. Y.K. and K.-Y.C. supervised, directed, and managed the study.

## Declaration of Competing Interest

The authors declare no conflict of interests.

## Data availability

Data will be made available on request. The data that support the findings of this study are available from the corresponding author upon reasonable request.

## Acknowledgements

This work was supported by National Research Foundation of Korea (NRF) grants funded by the Korean government (MSIP) (2019R1A2C3002751, 2020M3E5E2040018, and 2021R1A2C2093916) and a fund (2021-ER1001-01) by Research of Korea Centers for Disease Control and Prevention. M.Y. and H.K. were supported by the Brain Korea 21 (BK21) studentship from the National Research Foundation (NRF).

## Appendix A. Supporting information

Supplementary data associated with this article can be found in the online version at doi:10.1016/j.phrs.2023.106836.

## References

[1] C. Ballard, S. Gauthier, A. Corbett, C. Brayne, D. Aarsland, E. Jones, Alzheimer's disease, Lancet 377 (9770) (2011) 1019–1031.
[2] R. Brookmeyer, E. Johnson, K. Ziegler-Graham, H.M. Arrighi, Forecasting the global burden of Alzheimer's disease, Alzheimers Dement 3 (3) (2007) 186–191.
[3] K. Herrup, Reimagining Alzheimer's, disease–an age-based hypothesis, J. Neurosci. 30 (50) (2010) 16755–16762.
[4] W.A. Eimer, R. Vassar, Neuron loss in the 5XFAD mouse model of Alzheimer's disease correlates with intraneuronal Abeta42 accumulation and Caspase-3 activation, Mol. Neurodegener. 8 (2013) 2.
[5] D.J. Selkoe, J. Hardy, The amyloid hypothesis of Alzheimer's disease at 25 years, EMBO Mol. Med 8 (6) (2016) 595–608.
[6] L. Jia, J. Pina-Crespo, Y. Li, Restoring Wnt/beta-catenin signaling is a promising therapeutic strategy for Alzheimer's disease, Mol. Brain 12 (1) (2019) 104.
[7] D.C. Ryman, N. Acosta-Baena, P.S. Aisen, T. Bird, A. Danek, N.C. Fox, A. Goate, P. Frommelt, B. Ghetti, J.B. Langbaum, F. Lopera, R. Martins, C.L. Masters, R. P. Mayeux, E. McDade, S. Moreno, E.M. Reiman, J.M. Ringman, S. Salloway, P. R. Schofield, R. Sperling, P.N. Tariot, C. Xiong, J.C. Morris, R.J. Bateman, N. Dominantly Inherited Alzheimer, Symptom onset in autosomal dominant Alzheimer disease: a systematic review and meta-analysis, Neurology 83 (3) (2014) 253–260.
[8] S. Asher, R. Priefer, Alzheimer's disease failed clinical trials, Life Sci. 306 (2022), 120861.
[9] J. Cao, J. Hou, J. Ping, D. Cai, Advances in developing novel therapeutic strategies for Alzheimer's disease, Mol. Neurodegener. 13 (1) (2018) 64.
[10] R. Libro, P. Bramanti, E. Mazzon, The role of the Wnt canonical signaling in neurodegenerative diseases, Life Sci. 158 (2016) 78–88.
[11] E. Palomer, J. Buechler, P.C. Salinas, Wnt signaling deregulation in the aging and Alzheimer's Brain, Front Cell Neurosci. 13 (2019) 227.
[12] D.C. Lie, S.A. Colamarino, H.J. Song, L. Desire, H. Mira, A. Consiglio, E.S. Lein, S. Jessberger, H. Lansford, A.R. Dearie, F.H. Gage, Wnt signalling regulates adult hippocampal neurogenesis, Nature 437 (7063) (2005) 1370–1375.
[13] G.V. De Ferrari, M.E. Avila, M.A. Medina, E. Perez-Palma, B.I. Bustos, M. A. Alarcon, Wnt/beta-catenin signaling in Alzheimer's disease, CNS Neurol. Disord. Drug Targets 13 (5) (2014) 745–754.
[14] V. Budnik, P.C. Salinas, Wnt signaling during synaptic development and plasticity, Curr. Opin. Neurobiol. 21 (1) (2011) 151–159.
[15] L. Sommer, Q. Ma, D.J. Anderson, neurogenins, a novel family of atonal-related bHLH transcription factors, are putative mammalian neuronal determination genes that reveal progenitor cell heterogeneity in the developing CNS and PNS, Mol. Cell Neurosci. 8 (4) (1996) 221–241.
[16] S. Tutukova, V. Tarabykin, L.R. Hernandez-Miranda, The role of neurod genes in brain development, function, and disease, Front Mol. Neurosci. 14 (2021), 662774.
[17] X.Z. Yuan, S. Sun, C.C. Tan, J.T. Yu, L. Tan, The Role of ADAM10 in Alzheimer's Disease, J. Alzheimers Dis. 58 (2) (2017) 303–322.
[18] Y.C. Shang, Z.Z. Chong, S. Wang, K. Maiese, Wnt1 inducible signaling pathway protein 1 (WISP1) targets PRAS40 to govern beta-amyloid apoptotic injury of microglia, Curr. Neurovasc Res 9 (4) (2012) 239–249.
[19] S. Mehan, S. Bhalla, E.M. Siddiqui, N. Sharma, A. Shandilya, A. Khan, Potential roles of glucagon-like peptide-1 and its analogues in dementia targeting impaired insulin secretion and neurodegeneration, Degener. Neurol. Neuromuscul. Dis. 12 (2022) 31–59.
[20] J.Y. Vargas, M. Fuenzalida, N.C. Inestrosa, In vivo activation of Wnt signaling pathway enhances cognitive function of adult mice and reverses cognitive deficits in an Alzheimer's disease model, J. Neurosci. 34 (6) (2014) 2191–2202.
[21] C. Parr, N. Mirzaei, M. Christian, M. Sastre, Activation of the Wnt/beta-catenin pathway represses the transcription of the beta-amyloid precursor protein cleaving enzyme (BACE1) via binding of T-cell factor-4 to BACE1 promoter, FASEB J. 29 (2) (2015) 623–635.
[22] Q. Zeng, Z. Long, M. Feng, Y. Zhao, S. Luo, K. Wang, Y. Wang, G. Yang, G. He, Valproic acid stimulates hippocampal neurogenesis via activating the Wnt/beta-catenin signaling pathway in the APP/PS1/Nestin-GFP triple transgenic mouse model of Alzheimer's disease, Front Aging Neurosci. 11 (2019) 62.
[23] C. Hooper, R. Killick, S. Lovestone, The GSK3 hypothesis of Alzheimer's disease, J. Neurochem 104 (6) (2008) 1433–1439.
[24] C.H. Norgaard, S. Friedrich, C.T. Hansen, T. Gerds, C. Ballard, D.V. Moller, L. B. Knudsen, K. Kvist, B. Zinman, E. Holm, C. Torp-Pedersen, L.S. Morch, Treatment with glucagon-like peptide-1 receptor agonists and incidence of dementia: data from pooled double-blind randomized controlled trials and nationwide disease and prescription registers, Alzheimers Dement (N. Y) 8 (1) (2022), e12268.
[25] M. Gejl, A. Gjedde, L. Egefjord, A. Moller, S.B. Hansen, K. Vang, A. Rodell, H. Braendgaard, H. Gottrup, A. Schacht, N. Moller, B. Brock, J. Rungby, In Alzheimer's disease, 6-Month Treatment with GLP-1 analog prevents decline of brain glucose metabolism: randomized, placebo-controlled, double-blind clinical trial, Front Aging Neurosci. 8 (2016) 108.
[26] H.Y. Kim, J.Y. Yoon, J.H. Yun, K.W. Cho, S.H. Lee, Y.M. Rhee, H.S. Jung, H.J. Lim, H. Lee, J. Choi, J.N. Heo, W. Lee, K.T. No, D. Min, K.Y. Choi, CXXC5 is a negative-feedback regulator of the Wnt/beta-catenin pathway involved in osteoblast differentiation, Cell Death Differ. 22 (6) (2015) 912–920.
[27] S.H. Seo, E. Kim, Y. Joo, J. Lee, K.T. Oh, S.J. Hwang, K.Y. Choi, A mixed micellar formulation for the transdermal delivery of an indirubin analog, Pharmaceutics 12 (2) (2020).
[28] H. Oakley, S.L. Cole, S. Logan, E. Maus, P. Shao, J. Craft, A. Guillozet-Bongaarts, M. Ohno, J. Disterhoft, L. Van Eldik, R. Berry, R. Vassar, Intraneuronal beta-amyloid aggregates, neurodegeneration, and neuron loss in transgenic mice with

five familial Alzheimer's disease mutations: potential factors in amyloid plaque formation, J. Neurosci. 26 (40) (2006) 10129–10140.
[29] R. D'Hooge, P.P. De Deyn, Applications of the Morris water maze in the study of learning and memory, Brain Res Brain Res Rev. 36 (1) (2001) 60–90.
[30] H.Y. Kim, H.V. Kim, S. Jo, C.J. Lee, S.Y. Choi, D.J. Kim, Y. Kim, EPPS rescues hippocampus-dependent cognitive deficits in APP/PS1 mice by disaggregation of amyloid-beta oligomers and plaques, Nat. Commun. 6 (2015) 8997.
[31] R.G. Morris, P. Garrud, J.N. Rawlins, J. O'Keefe, Place navigation impaired in rats with hippocampal lesions, Nature 297 (5868) (1982) 681–683.
[32] P. Yan, X. Hu, H. Song, K. Yin, R.J. Bateman, J.R. Cirrito, Q. Xiao, F.F. Hsu, J. W. Turk, J. Xu, C.Y. Hsu, D.M. Holtzman, J.M. Lee, Matrix metalloproteinase-9 degrades amyloid-beta fibrils in vitro and compact plaques in situ, J. Biol. Chem. 281 (34) (2006) 24566–24574.
[33] F. Sarsoza, T. Saing, R. Kayed, R. Dahlin, M. Dick, C. Broadwater-Hollifield, S. Mobley, I. Lott, E. Doran, D. Gillen, C. Anderson-Bergman, D.H. Cribbs, C. Glabe, E. Head, A fibril-specific, conformation-dependent antibody recognizes a subset of Abeta plaques in Alzheimer disease, Down syndrome and Tg2576 transgenic mouse brain, Acta Neuropathol. 118 (4) (2009) 505–517.
[34] S. Jo, O. Yarishkin, Y.J. Hwang, Y.E. Chun, M. Park, D.H. Woo, J.Y. Bae, T. Kim, J. Lee, H. Chun, H.J. Park, D.Y. Lee, J. Hong, H.Y. Kim, S.J. Oh, S.J. Park, H. Lee, B. E. Yoon, Y. Kim, Y. Jeong, I. Shim, Y.C. Bae, J. Cho, N.W. Kowall, H. Ryu, E. Hwang, D. Kim, C.J. Lee, GABA from reactive astrocytes impairs memory in mouse models of Alzheimer's disease, Nat. Med 20 (8) (2014) 886–896.
[35] C.Y. Shao, S.S. Mirra, H.B. Sait, T.C. Sacktor, E.M. Sigurdsson, Postsynaptic degeneration as revealed by PSD-95 reduction occurs after advanced Abeta and tau pathology in transgenic mouse models of Alzheimer's disease, Acta Neuropathol. 122 (3) (2011) 285–292.
[36] D. Moechars, K. Lorent, B. De Strooper, I. Dewachter, F. Van Leuven, Expression in brain of amyloid precursor protein mutated in the alpha-secretase site causes disturbed behavior, neuronal degeneration and premature death in transgenic mice, EMBO J. 15 (6) (1996) 1265–1274.
[37] S. Jawhar, A. Trawicka, C. Jenneckens, T.A. Bayer, O. Wirths, Motor deficits, neuron loss, and reduced anxiety coinciding with axonal degeneration and intraneuronal Abeta aggregation in the 5XFAD mouse model of Alzheimer's disease, Neurobiol. Aging 33 (1) (2012) e29–e40, 196.
[38] S. Forner, S. Kawauchi, G. Balderrama-Gutierrez, E.A. Kramar, D.P. Matheos, J. Phan, D.I. Javonillo, K.M. Tran, E. Hingco, C. da Cunha, N. Rezaie, J. A. Alcantara, D. Baglietto-Vargas, C. Jansen, J. Neumann, M.A. Wood, G. R. MacGregor, A. Mortazavi, A.J. Tenner, F.M. LaFerla, K.N. Green, Systematic phenotyping and characterization of the 5xFAD mouse model of Alzheimer's disease, Sci. Data 8 (1) (2021) 270.
[39] R.G. Phillips, J.E. LeDoux, Differential contribution of amygdala and hippocampus to cued and contextual fear conditioning, Behav. Neurosci. 106 (2) (1992) 274–285.
[40] S. Choi, H.Y. Kim, P.H. Cha, S.H. Seo, C. Lee, Y. Choi, W. Shin, Y. Heo, G. Han, W. Lee, K.Y. Choi, CXXC5 mediates growth plate senescence and is a target for enhancement of longitudinal bone growth, Life Sci. Alliance 2 (2) (2019).
[41] S.H. Seo, E. Kim, M. Yoon, S.H. Lee, B.H. Park, K.Y. Choi, Metabolic improvement and liver regeneration by inhibiting CXXC5 function for non-alcoholic steatohepatitis treatment, Exp. Mol. Med 54 (9) (2022) 1511–1523.
[42] M. Kahn, Can we safely target the WNT pathway? Nat. Rev. Drug Discov. 13 (7) (2014) 513–532.
[43] D. Ferreira, L. Perestelo-Perez, E. Westman, L.O. Wahlund, A. Sarria, P. Serrano-Aguilar, Meta-review of CSF core biomarkers in Alzheimer's Disease: the state-of-the-art after the new revised diagnostic criteria, Front Aging Neurosci. 6 (2014) 47.
[44] M.V.F. Silva, C.M.G. Loures, L.C.V. Alves, L.C. de Souza, K.B.G. Borges, M.D. G. Carvalho, Alzheimer's disease: risk factors and potentially protective measures, J. Biomed. Sci. 26 (1) (2019) 33.
[45] J.M. Long, D.M. Holtzman, Alzheimer disease: an update on pathobiology and treatment strategies, Cell 179 (2) (2019) 312–339.
[46] C. Haass, D. Selkoe, If amyloid drives Alzheimer disease, why have anti-amyloid therapies not yet slowed cognitive decline? PLoS Biol. 20 (7) (2022), e3001694.
[47] M.A. Kling, J.Q. Trojanowski, D.A. Wolk, V.M. Lee, S.E. Arnold, Vascular disease and dementias: paradigm shifts to drive research in new directions, Alzheimers Dement 9 (1) (2013) 76–92.
[48] R. Nusse, H. Clevers, Wnt/beta-catenin signaling, disease, and emerging therapeutic modalities, Cell 169 (6) (2017) 985–999.
[49] G.V. De Ferrari, N.C. Inestrosa, Wnt signaling function in Alzheimer's disease, Brain Res Brain Res Rev. 33 (1) (2000) 1–12.